Reply to reviewers comments for: "Mechanical models to estimate the paleostress state from igneous intrusions" by Tara L. Stephens et al.

We thank both reviewers for their concise and constructive comments on the above manuscript. In almost all cases we have implemented the suggested changes. Below we present a full breakdown of the changes we have made, and our response to individual comments (original comment in black; response in blue). The main amendments to the manuscript are:

1) Introduction: Reviewer 1 suggested to provide more detail on why sills are typically omitted from paleostress analyses. This has been added: See L47-54.
2) Mechanical model (Figure 3): Reviewer 1 suggested to provide additional explanation for how changes in the stress regime, as well as changes in fluid pressure, affect the range of fracture attitudes that would dilate. We have added a short explanation to the manuscript to better explain this: See L155-163.
3) Fracture Mechanics: Reviewer 2 suggested that more explanation was required for the effect of pre-existing fractures on hydrofracture propagation. We have added a short section to address how pre-existing fractures that are oriented at a high angle to σ_3 can influence hydrofracture propagation: See L138-152.
4) Discussion: The discussion has been split into sub-sections and part has been re-written in a clearer and more concise style: See L275-315.

Reply to Reviewer 1

General Comments:
1) As discussed below, there may be potential for this method to be misapplied in the absence of detailed investigations of the timing and history of intrusive events, and the authors should explicitly discuss the critical field observations needed before applying the approach. The authors have previously done extensive and careful field work in this study area (e.g., Walker et al., 2017), so I believe the approach is valid for the San Rafael field. However, the method assumes that the stress field remains constant during emplacement of the measured intrusions, and thus the magnitude of fluid pressure (i.e., magma) is the critical parameter that determines the spread of the intrusion attitude data. With this in mind, the method also requires the emplacement of the measured intrusions, which exhibit a variety of attitudes, to be closely spaced in time (i.e., L137: "created during the same dilational event"). If one were to take this approach to a different field setting, it therefore may be misapplied if the timing of events is unknown.

So with this in mind; in contrast to the model presented in this study, what if the magnitude of the fluid pressure remained relatively low (thus restricting the range of intrusion attitudes at any given time and place), but the orientation of the stress field varied both temporally and spatially? Such a scenario would seem really likely under a classic cone sheet model for example.

The authors somewhat address this point on L 267-285, but I think a little more discussion is needed so that readers can explicitly see the potential pitfalls with the approach, and be shown how to deal with these with detail field observations and measurements. For example, what is unique about this study, compared to Jolly and Sanderson (1997), is that the authors also present the attitudes of fractures exhibiting compressional shear failure, thereby tightly bounding the

1

ellipse in the stereonets that provide constraints on fluid pressures. The interconnectivity between intrusions of different attitudes is also illustrated, suggesting they formed near-contemporaneously. I feel that careful measurements like these robustly support the model, and future studies could also consider this approach.

Reply: These are excellent points, our statement "created during the same dilational event" implies that intrusions with different attitudes will be either *mutually* cross-cutting, or linked together (e.g. our Figs 1 and 7). This is comparable to conjugate or orthorhombic fault sets where the mutual cross cutting relationships signify that the structures formed within the same stress state but not exactly at the same time. A lack of mutual cross cutting, or linking, relationships between intrusive sets would indicate that they represent separate events. Relative timings should therefore be identified in the field, and different intrusive sets, which will either represent different fluid pressures and/ or different stress states, should be recorded and analysed individually.

We have added in a short section that addresses these comments: See L155-163.

2) It would be useful for the reader to also have some quick background on why sills have been omitted from these types of paleostress analyses in the introduction. This could be included as a few sentences immediately after the comments on lines 46-48.

To me, this issue stems from the problem that (1) sills in many cases must be fed by dikes, and are often observed in regions which are thought to be extensional. Thus if we consider stress as the primary control on sill orientation, then the least compressive stress must be both vertical and horizontal in the region where sills are fed, which is often in an extensional setting. The effects of mechanical layering essentially act as a work-around for this paradox. (2) Sills are often observed intruding sedimentary layers, although this is no surprise as sedimentary layering is often horizontal. I know this group has brought up points such as these in recent papers, but I feel that it is important to bring these points to the forefront to provide broader context for the paper.

Reply: Thank you, we have added in a few lines to address this: See L47-54.

Specific Comments:

1) L 115: Please consider the terms "extensional" and "compressional" as the subject matter is intrusions rather than faults.

Reply: we see why Review 1 suggests this, however 'extensional' and 'compressional' refer to a strain and a stress, respectively; additionally these terms do not give a clear indication of principal stress axes orientation (e.g. horizontal extension and horizontal compression could both be used to describe a strike-slip regime). One of the key points of the manuscript is to show that intrusions (particularly sills) may be used as records of paleostress, in a similar fashion to faults. In the case of this study, thrust faults accommodate shortening either when there was no magmatic input, or in areas that did not become linked to a magmatic source; the sills are therefore representative of an otherwise thrust fault regime. We feel, therefore, that the association between intrusion attitudes and a given deformation regime is appropriate: L124 – 126 have been amended to *thrust-fault regime ($\sigma_v = \sigma_3$), strike-slip regime ($\sigma_v = \sigma_2$),* and *normal-fault regime ($\sigma_v = \sigma_1$).*

2) L 141-143: The other possibility is that it is multiple events where the orientation of the principle stresses has varied. I don't think this is the case in the paper, but it should not be overlooked. See Comment #1.

Reply: please see reply to comment General Comment 1.

3) L 162-163: No direct feeder relationships are observed, which is very rare in nature anyhow, but they have been inferred. For example, Figure 3 of Richardson et al. (2015) points to potential dike feeder based on sill thicknesses. Additionally, the thickness distributions of these sills do suggest potential NNE-SSE-trending feeders, which is parallel to the dikes (i.e., Walker et al., 2017). Finally, the Richardson et al. paper, which details the broad distribution of the sills in question, seems to be omitted from this study. It should be included and cited throughout accordingly.

Reply: Richardson et al. (2015) do infer a feeding relationship between the dikes and sills (their Figs. 2 & 3), however Walker et al. (2017) demonstrate at that for the Central Cedar sill location dikes cut thin sills, and the dikes within the volcanic breccia body have chilled contacts (their Fig. 5), which suggests that at that stratigraphic level the dikes and sills did not have a 'feeding' relationship. It is possible that both inferences are correct, in that the sills may have been fed by the dikes, but that transition from dike to sill was long-lived and involved several pulses of magma, with small enough volumes and/or enough time to form cooled contacts at the margin of the conduit. Since that observation is from the North of the San Rafael area, and the models and observations in the present study are limited to the south of the area, discussion of that locality is arguably beyond the scope of the paper. We have cited Richardson et al. (2015) where appropriate.

4) L 325: As suggested here and other locations in the text, the sills are often assumed to be intruding pre-existing structures when their attitudes are oblique to the principle stresses. What about faults and fractures generated at the propagation front of sills related to uplift of the overburden (e.g., Fig 7 of Thomson 2007)? I don't think these would count as pre-existing, but would be oblique to the least compressive stress, and thus fit with the model presented. Note that they don't have to be as high-angle as the ones in the figure referred to.

Reply: This is a very good point, but we feel that it is effectively unknowable with the current field data. At present it is not possible to constrain whether these are truly "existing" fractures, or whether they are faults/fractures formed ahead of the propagating tip. Further detailed analysis of fracture populations around the intrusions, at the regional and local scale, may provide some useful information as to whether the fracture attitudes are local to sills, but from our existing data set, this appears not to be the case, and further, it may not be possible to distinguish different and superimposed populations anyway. Analysis of fracture/fault slip distributions ahead of sill tips may give some further insights to the problem, assuming that the fractures have distinguishable slip distribution profiles depending on whether they are pre-existing or newly-generated. Distinguishing displacement maxima and/or slip distribution profiles for dykes may be possible because of the potential abundance of offset markers, and likewise for steep faults/fractures, as with those shown in Thomson (2007). In a field study of sills, this would require excavation of the fracture sets; we have not done this, and it is unclear whether this information would be preserved at any useable scale and quantity owing to the gentle dips of the fractures, and the lack of offset markers.

We have added an additional section which describes the conditions necessary for dilation of high-angle fractures: See L138-152.

5) Figure 1: Change normal fault regime, to "extensional regime". Change thrust fault regime to "compressional regime". We are focusing on intrusions in this paper, and not faults.

6) Figure 3: Same as figure 1. Change to "extensional regime", "strike-slip regime", and "compressional regime".

Also, I think in this figure there needs to be a little more explanation in the caption.

From my understanding, if the pole to the fracture plane is situated in a certain color portion of the stereonet, then the "color" indicates the opening angle (_). So if the pole of the fracture plane is in a black region, it will have an opening angle between 80-90 degrees (and subsequently a large true thickness). If the pole of the fracture plane is in a yellow regime, it will have an opening angle between 0-10 degrees, and have a smaller true thickness.

I doubt this is intuitive to most readers looking only at this figure, and I think the paper would benefit from taking the time to explain it in greater detail, perhaps using an example like I did above. [Note, I noticed later that the text discusses poles to planes, but I still think it should be explained first thing when the reader first views the caption.]

Reply to comments 5 & 6: Please see reply to Specific Comment (1).

The caption of Fig. 3 has been expanded to explain the relationship between the colour contouring, opening angle, and intrusion thickness.

Recommend references
Richardson, J. A., Connor, C. B., Wetmore, P. H., Connor, L. J., & Gallant, E. A. (2015).
Role of sills in the development of volcanic fields: Insights from lidar mapping surveys of the San Rafael Swell, Utah. Geology, 43(11), 1023-1026.

Thomson, K. (2007). Determining magma flow in sills, dykes and laccoliths and their implications for sill emplacement mechanisms. Bulletin of Volcanology, 70(2), 183-201.

Reply: Thank you for the suggestions, Richardsson et al. (2015) has been cited where appropriate. We have used an alternative paper (Malthe-Sørenssen et al., 2004) to refer to the emplacement of saucer-shaped sills.

Reply to Reviewer 2:

Major comments:
Despite being short, I think the paper lacks references especially on the role of pre-existing fractures on magma intrusions, and on the mechanics of fracture propagation. Line 328: "Failure of intact rock requires a higher fluid pressure than for reactivation of pre-existing structures". I don't agree with that. As you said yourself in the paper it depends on the magma pressure and the orientation of the fractures, as well as if it sealed or not. In addition, the propagation of the tip of a crack would tend to have a fracture to not reopen pre-exiting ones due to their angular orientations with the local stress (or maybe on short distance [Gaffney et al., 2007]).

Reply: Thank you for pointing this out, we agree and Lines 328 – 333 have been removed. Additionally, we understand why Reviewer 2 suggests to include fracture mechanics literature, however the model proposed here does not refer to hydrofracture initiation or propagation; it simply calculates the opening angle for fractures that were linked to the fluid system. We have added in a short section to address how pre-existing fractures that are oriented at a high angle to σ_3 can influence hydrofracture propagation: See L138-152.

Additional references have also been added into the paper regarding the geometry of extensional-shear fractures formed via failure of intact rock: Hancock, 1985; Sibson, 1996; and Ramsey and Chester, 2004.

Minor comment: Line 57: "dilation of a fluid-filled pre-existing: : :". I think there is a mistake here. I don't believe you mean to dilate a fracture with liquid in it?

Reply: Correct: "fluid-filled" has been changed to "cohesionless".

Recommend references

Gaffney, E. S., B. Damjanac, and G. A. Valentine (2007), Localization of volcanic activity: 2. Effects of pre-existing structure, Earth and Planetary Science Letters, 263(3-4), 323-338.

Reply: Thank you for the suggestion, the reference has been cited where appropriate.

Mechanical models to estimate the paleostress state from igneous intrusions

Tara L. Stephens[1], Richard J. Walker[1], David Healy[2], Alodie Bubeck[1], Richard W. England[1]

[1] School of Geography, Geology and the Environment, University of Leicester, Leicester, LE1 7RH, UK
[2] School of Geosciences, King's College, University of Aberdeen, Aberdeen, AB24 3UE, UK

Correspondence to: Tara Stephens (tls15@le.ac.uk)

Abstract

Dikes and sills represent an important component of the deformation history in volcanic systems, but unlike dikes, sills are typically omitted from traditional paleostress analyses in tectonic studies. The emplacement of sheet intrusions is commonly associated with mode I fracturing in a low deviatoric stress state, where dilation is perpendicular to the fracture plane. Many natural examples of sills and dikes, however, are observed to accommodate minor shear offsets, in addition to a component of dilation. Here we present mechanical models for sills in the San Rafael Subvolcanic Field, Utah, which use field-~~derived~~ based measurements of intrusion attitude and opening angles to constrain the tectonic stress axes during emplacement, and the relative magma pressure for that stress state. The sills display bimodal dips to the NE and SW and consistent vertical opening directions, despite variable sill dips. Based on sill attitude and opening angles, we find that the sills were emplaced during a phase of NE-SW horizontal shortening. Calculated principal stress axes are consistent (within ~4°) with paleostress results for penecontemporaneous thrust faults in the area. The models presented here can be applied to any set of dilational structures, including dikes, sills, or hydrous veins, and represent a robust method for characterising the paleostress state in areas where other brittle deformation structures (e.g. faults)~~,~~ are not present.

1 Introduction

Sills and dikes are traditionally treated as extension fractures with a dilation vector normal to the fracture wall, i.e. they are extension fractures (*Mode I,* e.g. Anderson, 1951). This assumption has important implications for the use of sheet intrusions in constraining tectonic stress states, because ~~extension fractures dilate in the direction of~~ the minimum compressive

stress (σ_3) is perpendicular to the extension fracture walls; local deflections of the intrusion

attitude are commonly inferred to represent local rotations of the stress axes. This is most

commonly attributed to mechanical layering, and the presence of pre-existing structures (e.g.

Rubin, 1995; Gudmundsson, 2002; 2011a; Magee et al., 2016). This model implies that

intrusions can locally propagate out of the regional σ_1–σ_2 plane, via Mode I failure of intact

rock, or through Mode I dilation of pre-existing structures, producing intrusions that display

variable dilation vectors along a single intrusion. Notably, many field examples of sills and

dikes exhibit near-parallel dilation vectors, regardless of the intrusion attitude (e.g. Hoek, 1991;

Walker, 1993; Airoldi et al., 2011; Martinez-Poza et al., 2014; Muirhead et al., 2014; Eide et

al., 2016; Walker et al., 2017). Intrusions that demonstrate shear-offset of markers across their

margins indicate that during emplacement the dilation vector was inclined from plane-normal

(Muirhead et al., 2014; Stephens et al., 2017; Walker et al., 2017); this obliquity of opening

can be characterised by the opening angle (**Fig. 1**).

Dilated structures have been studied in detail by Delaney et al. (1986), Baer et al. (1994)

and Jolly and Sanderson (1997), who applied mechanical methods to estimate paleostress states

using sheet intrusion attitudes. These mechanical models have been adopted for statistical

constraints on paleostress axes, and the paleostress state, from vein or dike data (e.g. Sato et

al., 2013; Yamaji, 2016). Although several methods exist to determine paleostress axes, and a

state of paleostress via fault, fracture, or dike data, subhorizontal sheet intrusions (sills) are

typically omitted from such analyses. This is because sill emplacement is commonly associated

with a local rotation of the principal stress axes, as a result of bedding or other layer

heterogeneities, during regional extension or a low-deviatoric stress state (i.e. where $\sigma_1 \approx \sigma_2 \approx$

σ_3; e.g. Gudmundsson, 2011a; Magee et al., 2016). Several studies have demonstrated that sills

may also form during tectonic horizontal shortening, where the minimum principal stress is

vertical (Walker, 2016; Walker et al., 2017; Stephens et al., 2017); hence sills can be used as

paleostress indicators, provided they are accompanied by detailed kinematic characterisation.

Here, we present mechanical models, based on those of Jolly and Sanderson (1997), to

determine paleostress state using the attitude of dilated fracture sets; we verify this using the

measured opening angle of the intrusions. The method is applicable to any dilated fracture;

here we focus on the stress state associated with sill emplacement in the San Rafael

Subvolcanic Field, Utah, and compare these results to fault data in the same area, to

demonstrate the particular importance of subhorizontal igneous intrusions as records of paleostress.

65 ~~3~~2 Dilation of pre-existing fractures

Dilation of a cohesionless~~fluid-filled,~~ pre-existing~~,~~ planar structure occurs when the fluid pressure (P_f) exceeds the normal stress on the plane (σ_n; **Fig. 1**) (Delaney et al., 1986; Jolly and Sanderson, 1997). Normal stress is related to the plane attitude (θ), and the maximum (S_H) and minimum (S_h) principal stresses acting on the plane (Jolly and Sanderson, 1997):

70 $$\sigma_n = \frac{S_H + S_h}{2} + \frac{S_H - S_h}{2} cos2\theta, \tag{1}$$

with the range of possible dilatant fracture attitudes controlled by the stress ratio (ϕ),

$$\phi = \frac{\sigma_2 - \sigma_3}{\sigma_1 - \sigma_3}, \tag{2}$$

and the driving pressure ratio (R') (Baer et al., 1994):

$$R' = \frac{P_f - \sigma_3}{\sigma_1 - \sigma_3}. \tag{3}$$

75 The stress ratio, ϕ, is a non-directional value that describes the relative magnitudes of the principal stresses: $\sigma_3 \leq \sigma_2 \leq \sigma_1$ (here, compressive stresses are positive). The driving pressure ratio R' describes the relative magnitudes of the fluid pressure and the remote stress state: When $R' < 0$ (i.e., $P_f \leq \sigma_3$) there is no dilation, and when $R' \geq 1$ (i.e., $P_f \geq \sigma_1$) all fracture attitudes could dilate. This assumes that an intrusion is emplaced during a deviatoric stress state (i.e. where $\sigma_1 \neq \sigma_2 \neq \sigma_3$); ~~whereas,~~ if $P_f > \sigma_3$ during a non-deviatoric stress state (i.e. where $\sigma_1 = \sigma_2 = \sigma_3$), all pre-existing fracture attitudes could dilate.

Pre-existing fractures, with poles parallel to the σ_3 axis, will show plane-normal dilation (i.e. dilation parallel to the normal stress vector). Fractures inclined to the plane of σ_3 resolve a shear stress on their surface (Delaney et al., 1986). During dilation, shear stress is reduced to

85 zero through a plane-oblique dilation vector (~~extensional shear~~extensional-shear). The angle between the dilation vector and normal stress is defined as the opening angle (μ; **Fig. 1a-c**) and represents the ratio of shear to dilation (Delaney et al., 1986). ~~Extensional shear~~Extensional-

8

shear therefore acts to reduce the amount of dilation. For an intrusion comprising inclined and ~~sub-horizontal~~subhorizontal sections, the inclined sections will therefore be thinner than ~~sub-horizontal~~subhorizontal sections oriented perpendicular to σ_3 (e.g. **Fig. 1c, d**) for a given fluid pressure, providing the stress state is deviatoric and $0 < R' < 1$ (England, 1988). The dilation vector can be measured using traditional compass techniques in the field based on offset piercing points or unique contact geometries, such as recognisable corners in the intrusion walls (e.g. **Figs 1c, 2a, b**). True offsets result from ~~extensional shear~~extensional-shear opening (**Fig. 2c, d**), however apparent shear offset can be produced by marker units that are oriented at an oblique angle to the intrusion plane (**Fig. 2e**~~);~~), or via dilation of pre-existing faults, which produce a larger than expected opening angle (**Fig. 2f**). To determine whether offset and the opening angle is true, or apparent, multiple manual measurements of opening angle and intrusion thickness must be made along strike of an intrusion (**Figs 1c, 2g**). The opening angle (μ) of a dilated fracture can be calculated as the inverse cosine of the true thickness (t, normal to the plane) and the vertical thickness (tv, parallel to the dilation vector; **Fig. 1c**):

$$\mu = \cos^{-1}(t/tv). \tag{4}$$

Alternatively, μ can be measured as a rake of the obtuse angle between the intrusion contact and the dilation vector, minus 90°. Importantly, this measurement only accounts for the opening angle in two dimensions, movement in or out of the face will not be recorded; therefore dip-parallel sections should ideally be used.

The opening angle is related to the shear stress (τ), normal stress (σ_n), and fluid pressure (P_f) acting on that plane at the time of intrusion (Delaney et al., 1986; Jolly and Sanderson, 1997):

$$\mu = \tan^{-1}\left(\frac{\tau}{P_f - \sigma_n}\right). \tag{5}$$

Equation 5 shows that if the fluid overpressure ($P_f - \sigma_n$) is equal to the shear stress, the opening angle is 45°, and the shear to dilation ratio is unity~~dilation is equal to shear displacement~~. If the overpressure is greater than the shear stress, the opening angle is less than 45°, and the fracture will show a greater component of dilation to shear. When μ is negative, the fracture will remain closed as the fluid pressure did not exceed the normal stress. An intrusive segment, however, may inflate against a closed fracture (where $P_f < \sigma_n$), causing a local contractional shear, and a blunt intrusion tip (e.g. **Fig. 2g**).

9

53 Mechanical models for fracture dilation and opening angle

Equation 5 can be ~~visualised~~ represented in ~~three~~ three-dimensional (3D) space, for any given stress state, stress ratio and fluid pressure~~.~~: Figure 3 shows the opening angle (μ) of all possible fracture planes in 3D space, plotted as colour-contoured pole to plane values of μ, on equal area lower hemisphere stereographic projections and on 3D Mohr ~~Circles~~Diagrams. Fluid pressure was calculated at five equal intervals relative to the ambient stress state, which are expressed as *R'* values (**Fig. 3a**). Figure 3 shows plots of opening~~Opening~~ angles ~~are plotted~~ for three tectonic regimes where ϕ is 0.5: (1) a thrust-fault regime ($\sigma_v = \sigma_3$)~~thrust~~ (**Fig. 3b**); (2) a strike-slip regime ($\sigma_v = \sigma_2$)~~strike slip~~ (**Fig. 3c**); and (3) a normal-fault regime ($\sigma_v = \sigma_1$)~~normal faults~~ (**Fig. 3d**). The principal stress attitudes are constant in all models, with the azimuth for the maximum horizontal stress~~compression~~ (σ_H) trending E-W. All planes are modelled as cohesionless surfaces.

The models complement the results of Jolly and Sanderson (1997), and demonstrate that within a given stress state, increasing the fluid pressure increases the range of pre-existing fracture attitudes that can dilate, provided the dilated fracture is linked to the magmatic source. The models also show that for any given fracture, increasing P_f decreases μ. Where $\sigma_3 < P_f \leq \sigma_2$ (**Fig. 3b-d, i–ii**), the dilation zone, delineating the poles to fractures that are predicted to dilate, forms an ellipse about the σ_3 axis and is elongate in the direction of the intermediate stress (σ_2); only fractures with poles parallel to the σ_3 axis show Mode I opening. If $\sigma_2 < P_f < \sigma_1$ (**Fig. 3biii-diii**) the dilation zone forms a girdle parallel to the axis of σ_2, with two defined zones of near Mode I opening (0-10º) surrounding the σ_2 and σ_3 poles. Fractures of all attitudes ~~will~~ can dilate if $P_f = \sigma_1$ (**Fig. 3biv-div**). The models suggest that Mode I opening of pre-existing fractures should only be common if the fluid pressure exceeds σ_1 (e.g., **Fig. 3bv-dv**). For dilation of misoriented cohesionless fractures, with planes oriented at a high angle to σ_3, a higher fluid pressure is required to overcome the normal stress acting on their surface (e.g. Gaffney et al., 2007). Importantly, if misoriented planes do not become linked to the fluid network, high fluid overpressures will be relaxed by dilation of preferentially oriented pre-existing structures, or via failure of intact rock (e.g. Sibson, 2012). Dilational fracture data should therefore plot stereographically with the greatest density of poles to planes about the σ_3 axis (Jolly and Sanderson, 1997; Yamaji et al., 2010). Propagating intrusions may cut across or terminate

against misoriented structures, which plot in the zone of no dilation (white areas on the Mohr circles and stereonets; **Fig. 3**), as the normal stress acting on these planes exceeds the fluid pressure, preventing dilation (e.g. Gaffney et al., 2007; Gudmundsson, 2011a). Terminated intrusions may inflate against closed fractures if magma supply continues; dilation will be accommodated by local shear along the closed fracture producing a blunt intrusion tip (Baer, 1991; Stephens et al., 2017). Through measurement of ~~Therefore, by measuring~~ the opening angles of veins or intrusions, and determining the distribution of fracture attitudes that are in contact with intrusions, but ~~were~~ not dilated, it is therefore possible to constrain the fluid pressure relative to the ambient stress state. ~~It is important to note that pre-existing fractures must become linked to the magmatic system in order for them to be dilated and intruded; where the normal stress acting on a fracture, which is in contact with an intrusion, exceeds the fluid pressure, the fracture will not dilate, but the intrusion may inflate against it, creating a blunt tip ($\mu=90°$) (Stephens et al., 2017). Therefore, by measuring the opening angles of veins or intrusions, and determining the distribution of fracture attitudes that are in contact with intrusions but were not dilated, it is possible to constrain the fluid pressure relative to the ambient stress state. Here, we have applied this method to igneous sills in the San Rafael Subvolcanic Field, Utah (SRSVF).~~

In addition to changes in fluid pressure, fracture dilation is also sensitive to changes in remote stress, particularly at lower P_f. For instance, where $\sigma_3 < P_f \leq \sigma_2$ (**Fig. 3b-d, i–ii**) each stress regime is defined by a particular range of fracture attitudes, with a unique opening angle pattern. Where $\sigma_2 < P_f \leq \sigma_1$ (**Fig. 3b-d, iii–iv**), the thrust-fault regime (**Fig. 3b_{iii-iv}**) and strike-slip regime (**Fig. 3c_{iii-iv}**) have similar opening angle patterns, whereas the distribution of attitudes and opening angles for the normal-fault regime (**Fig. 3d_{iii-iv}**) is unique. Applied carefully, using detailed kinematic field analyses of sills, and their associated deformation, the method has the potential to discriminate between intrusions related to different remote stress states. Here, we have applied this method to igneous sills in the San Rafael Subvolcanic Field, Utah (SRSVF).

Dilated fractures, created during the same dilational event, will produce a unique distribution of opening angles when plotted stereographically as poles to planes (e.g. Jolly and Sanderson, 1997; Yamaji et al., 2010; Stato et al., 2013). Whether this is a tight cluster or a distributed set of poles, the pattern is usually interpreted to represent a single event, governed by one fluid pressure (e.g. Jolly and Sanderson, 1997); however, it is possible that the data represents multiple events caused by fluid pressure pulses of varying magnitude (Yamaji et al.,

11

2010). As the opening angle represents the ratio of shear to dilation (Delaney et al., 1986), magmatic events of varying magnitude, within the same governing stress state, could produce cross-cutting intrusions with similar geometries, but different opening angles (e.g. **Fig. 3**). The attitude and opening angle of dilated fractures, along with cross-cutting relationships, can therefore be used to identify whether a network of dilated fractures represents one, or multiple, fluid pressure pulses and the stress state during each pulse.

64 Stress state model for sill emplacement: San Rafael Subvolcanic Field

The San Rafael Sub Volcanic Field (SRSVF) is located in the north-western Colorado Plateau, central Utah (**Fig. 4a**), and comprises numerous, sills, dikes and volcanic breccia bodies (**Fig. 4b, c**). The close spatial association between these different intrusive bodies has been suggested to reflect emplacement during a low deviatoric stress state (Delaney and Gartner, 1997; Richardson et al. 2015). no No crustal magma chambers have been identified as the source for the intrusive complex (Delaney & and Gartner, 1997). The exposed intrusive system was emplaced at ~1 km depth, within the Mid Jurassic sedimentary rocks of the San Rafael Group, which comprises four formations; the Carmel Formation (siltstone and shale), Entrada Sandstone (interbedded sandstone, siltstone and claystone), Curtis Formation (interbedded glauconitic sandstone, and siltstone), and the Summerville Formation (siltstone, sandstone and shale) (Gartner, 1986; Richardson et al., 2015). The sequence represents a paralic environment, with near-shore and shallow marine deposits (Gartner, 1986; Peterson, 1988). The sills are mainly emplaced within the Entrada Sandstone, however they also cut across formation boundaries to intrude the Carmel and Summerville Formations (e.g. **Fig. 4d**; Walker et al., 2017). Richardson et al., (2015) highlighted an example of a dyke-to-sill transition for the Cedar Mountain sills (**Fig. 4b**). Our study focuses on sills in the southern SRSVF (**Fig. 4b**), and we cannot confirm that relationship here. In our study area, Ssills and dikes display mutual cross-cutting relationships, but no feeding relationships have been observed (e.g. **Fig. 4e**; Gartner, 1986; Walker et al., 2017), and we have observed no dyke-sill transitions for the major sills (e.g., **Fig. 4c**). Delaney and Gartner (1997) determined ages of dike emplacement between 4.6 and 3.7 Ma; the field relationships therefore constrain sill emplacement to a ~1 Myr interval.

Walker et al. (2017) interpret the sills in the SRSVF as low-angle conjugate intrusions, and concludedthey show that the sills record a phase of horizontal tectonic shortening, rather

12

215 than relating to local deflections due to material layering. The sills range from <10 cm to ~30 m thick, and are discordant to bedding, with dips of 1 – 25º (**Fig. 4d, f**). Based on sill attitude measurements over km-scale outcrops, Walker et al. (2017) showed that sill poles cluster about a near-vertical axis with two defined clusters: a NW and SE dipping set in the northern SRSVF, and a NE and SW dipping set in the southern SRSVF. This study focuses on the NE and SW

220 dipping sills in the southern SRSVF (**Fig. 4b, c**).

Across all scales, we find mutual cross-cutting relationships between sills with bimodal dips (e.g. **Figs 1c, 5a-c**), and en echelon sill segments which define low-angle (~20º dip) conjugate sets (**Fig. 5a**). Deformation bands and gypsum veins have comparable attitudes to sills and thrust faults in the field area, and define low-angle conjugate sets with NE and SW

225 dips (**Fig. 5d-i**). Sills intruded, and ~~are~~ have been cut by, low angle fractures, thrust faults and reverse faults (all referred to as thrust faults from ~~hereon in~~henceforth), and either cut or abut against sub-vertical fractures (**Figs 4d, 5f**; Walker et al., 2017). A constant near-vertical opening direction is noted across all sill segment attitudes (**Figs 6, 7a**). Local sill contact data displays a range of dips from (4° - 87°) with horizontal to subhorizontal sill segments (0-20°

230 dip) showing plane-normal (Mode I) and ~~extensional shear~~extensional-shear dilation ($\mu = 0$-20°), respectively (**Fig. 6a, 7a**). Inclined segments (20-56° dip) are consistently thinner than adjoining horizontal segments and display reverse-sense shear offset of piercing points ($20° < \mu \lesssim 75º$; **Fig. 7a**). Subvertical to vertical fractures (>70º dip) were not intruded (**Fig. 7a**) suggesting that fluid pressure was less than the normal stress on those planes during intrusion,

235 and the opening angle was $< 0°$.

Since the range of dilated sill attitudes is known, we can determine the relative stress and fluid pressure, using the parameters ϕ and R'. We calculate these parameters stereographically, using an ~~amended~~adapted method from Jolly and Sanderson (1997). The local sill contact data are plotted as poles to planes and coloured by their µ-value; the pole

240 cluster showing Mode I opening (µ=0-10º) is fitted with an ellipse (**Fig. 7b**). For data with a clustered distribution, this ellipse geometry provides a guide for the total range of dilated fractures, where blunt tips define the limit of fracture attitudes able to dilate; beyond this is the zone of no opening (where µ<0°; **Fig. 7b**). The minimum compressive stress (σ_3) plots in the centre of the Mode I ellipse (which likely coincides with the centre of the data cluster); σ_1 and

245 σ_2 are mutually orthogonal to this (**Fig. 7c**). If the data has a girdled distribution, the 0-10° ellipse should be used as an approximation for the geometry of the zone of no opening. In these cases, there will be two clusters of poles where µ=0-10° (see **Fig. 3b_{iii}-d_{iii}**), the larger ellipse

13

signifies the location of σ_3. A distributed set of dilated fractures may contain several zones of Mode I opening (μ=0-10°; see **Fig. 3**): σ_3 will plot in the larger of these ellipses and σ_1 in the zone of highest opening angle, or the smallest Mode I ellipse when P_f exceeds σ_1 (see **Fig. 3b$_v$-b$_v$**).

Field data for sills in the SRSVF can be fitted to an elliptical region on the stereonet with a NW-SE long axis (**Fig. 7b**), giving horizontal NE-SW maximum compression where: σ_1 plunges 3° towards 068°; σ_3 is vertical, plunging 87° towards 265°; and σ_2 is horizontal plunging 1° towards 158° (**Fig. 7c**). Using the stereonet data in **Figure 7c** we derive the angles θ_1 and θ_2 which are used to calculate the stress ratio (ϕ) and driving pressure ratio (R') by Jolly and Sanderson (1997):

$$\phi = \frac{1+\cos(2\theta_2)}{1+\cos(2\theta_1)}, \tag{6}$$

and

$$R' = \frac{1+\cos(2\theta_2)}{2}, \tag{7}$$

where θ_1 is the angle between the σ_2 axis and the perimeter of the dilational ellipse and θ_2 is the angle between the σ_1 axis and the dilational ellipse (Jolly and Sanderson, 1997). When an ellipse can only be fit~~ted~~ to the zone of no dilation, Jolly and Sanderson (1997) provide an alternative method for calculating ϕ. The R'-value is ~~two~~ two-dimensional (2D); it does not take into account the magnitude of σ_2. The ~~three~~ three-dimensional relationship between the fluid pressure and all principal stresses is illustrated by the ellipse geometry on the stereonet (**Fig. 7c, d**), and can also be visualised through construction of a 3D Mohr circle (**Fig. 7e**).

The calculated ϕ (0.77) and R' (0.68) values define the stress ratio and driving stress used to create the opening angle mechanical model (**Fig. 7d**). For the model, we assigned a minimum, vertical stress of 25 MPa to simulate a ~1 km emplacement depth (Gartner, 1986). Development of ~~extensional shear~~extensional-shear fractures requires a low differential stress (σ_D: $\sigma_1 - \sigma_3$): $4T$ ~~>~~≤ $\sigma_D < 5.66T$; compressional shear faults require that σ_D >5.66T (T is the host rock tensile strength; Sibson, 2003). Due to the bimodal (conjugate) dip distribution of the sills, their consistent near-vertical opening direction, and the mutual cross-cutting and intrusive relationship between thrust faults and sills we estimated that $\sigma_D = 6T$. We estimate the tensile strength of the host rock at 1 km depth to be 3 MPa, giving $\sigma_D = 18$ MPa~~;~~. It should be noted, however, that~~though~~ due to the nature of the model, providing all parameters are scaled relative

to T, the value of T does not change the resulting opening angle pattern, only the ~~relative~~ magnitudes of the principal stresses and fluid pressure. ϕ (0.77) and R' (0.68) derived in the model indicate a mild horizontal radial compression during emplacement, with fluid pressure less than σ_2 (**Fig. 7d, e**).

The measured opening angles of the studied sills fit with the contouring of a single ellipse (**Fig. 7d**), suggesting that during the intrusion of ~~the~~ sills in the study area, the fluid pressure and stress state remained relatively constant~~.; however~~However, we acknowledge that a broader study across the SRSVF may reveal spatio-temporal fluctuations in either the stress ~~state~~ regime or magma pressure.

5   Discussion

5.1   Sill geometry as a record of far-field stress

~~7   Sill geometry as a record of stress~~

Sills in the SRSVF are mildly transgressive, in that although they have intruded parallel to bedding at a local scale (e.g., **Fig. 5b, c, f**), at the field-scale they cut across the stratigraphy at a low angle (**Figs 4d and 5a-b**; Walker et al., 2017). Transgressive sill geometries are typically inferred to represent either the peripheral section of a saucer-shaped sill (e.g., Malthe-Sørenssen et al., 2004), or a low-angle cone sheet emanating from a magma chamber (e.g. Gudmundsson, 2006; Martí and Geyer, 2004). In either case, the transgressive segments should have an overall centripetal dip distribution. No magma chamber has been identified in the SRSVF, and the sills do not dip towards a central source, nor do they have a saucer-shaped geometry. Sills in the SRSVF show consistent bimodal dip patterns, with mutual cross-cutting relationships, at the outcrop to field scale (i.e. for sills that are centimetres- to tens-of-metres thick). We infer, as noted by Walker et al. (2017), that the bimodal sill geometry is representative of low-angle conjugate faults, which required a deviatoric stress state ($\sigma_D >$ 5.66T; Sibson, 2003) during emplacement.

At the local (cm - m) scale, the SRSVF sills display a range of attitudes with consistent vertical opening directions, and attitude-dependent thickness variations. In a low-deviatoric stress state, local variations in intrusion attitude are traditionally inferred to represent rotations of the principal stress axes, which may be caused by the effects of mechanical layering (e.g.

15

Gudmundsson, 2011a), or pre-existing faults and fractures (e.g. Fossen, 2010; Magee et al., 2013). Local stress rotations would therefore cause intrusions of any attitude to dilate in a Mode I sense, producing a polymodal distribution of opening directions across an intrusive suite. In that case, the aperture (true thickness) of the segment would be dominantly controlled by the host rock elastic properties (mainly Young's Modulus, E) (e.g. Brenner and Gudmundsson, 2004). Units with low E are less stiff than those with high E; i.e., a low E material will accrue more strain for a given stress. Accordingly, when a fluid-filled fracture, with constant fluid pressure, cross-cuts units with varying elastic properties, it will have a larger aperture in units with low E, and a smaller aperture in units with higher E (Brenner & Gudmundsson, 2004; Gudmundsson, 2011b). Local attitude variations of the SRSVF sills do not correspond solely to bedding interfaces. Although we infer that the inclined sill sections are dilated pre-existing fractures, the consistent vertical opening directions suggests that inclined fractures were subject to extensional-shear, rather than Mode I, dilation. This is supported by the attitude-dependant (rather than lithology-dependent) thickness variations; horizontal sill segments are consistently thicker than adjoining inclined segments, regardless of the hosting lithology.

Areas that host several intrusion sets, with different attitudes, are commonly interpreted to represent discrete and separate intrusive events (e.g. Delaney and Gartner, 1997; Walker, 1993). Our study, however, suggests that the observed range of sill attitudes is indicative of magmatism during a deviatoric far-field stress state (e.g., Walker, 2016; Walker et al., 2017). The sills may, therefore, be equivalent to reverse faults in the area, accommodating horizontal shortening, and vertical thickening.

~~Intrusions are typically treated as hydrofractures that formed in a low deviatoric far-field stress state (i.e. where $\sigma_1 \approx \sigma_2 \approx \sigma_3$), where the magma pressure exceeded the minimum compressive stress plus the host rock tensile strength (i.e. $P_f \geq \sigma_3 + T$; e.g. Gudmundsson, 2002; Kavanagh et al., 2006). For such a case, it should be possible to dilate pre-existing cohesionless fractures of all attitudes in a Mode I sense, and fractures of all attitudes should have similar apertures (true thickness). In a deviatoric stress state (i.e. where $\sigma_1 \neq \sigma_2 \neq \sigma_3$), the aperture of a fluid-filled fracture is influenced by its attitude relative to the principal stress axes, the fluid overpressure ($P_f - \sigma_n$) within the fracture, and the host rock elastic properties (Young's modulus, E, and Poisson's ratio, ν), at the time of dilation (e.g. England, 1988; Gudmundsson, 2011b). As noted in Section 2, fractures that are oriented parallel to the σ_1-σ_2 plane (perpendicular to the σ_3-axis) will have a greater thickness than those oriented obliquely to the~~

340 σ_1-σ_2 plane (for a given fluid pressure), as the fluid overpressure required to cause dilation must also relax the shear stress on an inclined surface. Material elastic properties control how the host rock responds to an applied stress: Units with high E are less compressible than those with low E. Therefore, if a fluid-filled fracture with constant fluid pressure, cross-cuts units with varying elastic properties, the fracture will have a larger aperture in units with low E, and a

345 smaller aperture in units with higher E (Gudmundsson, 2011b). The studied sills in the SRSVF predominantly intrude Entrada sandstone units and display along-strike changes in attitude; thinner inclined sections and thicker horizontal sections (**Figs 5a-c, 6, 7a**). These variations of attitude and thickness do not correspond to bedding interfaces, or lithological changes in the host rock. Sharp contacts between cross-cutting sills suggest that older sills were solidified

350 prior to intrusion of the younger sills (**Fig. 6**). As such, contrasts in elastic properties between the older sills and the sandstone could have promoted thickness variations in the younger sills, however, where sills are cross-cutting, the younger sills maintain a constant thickness when they are near-horizontal; thickness changes are only associated with inclined sections (**Fig. 6**). We infer that for the sills in the SRSVF detailed in our study, along-strike thickness variations

355 are controlled by the segment attitude, the far-field stress state, and the fluid pressure, rather than host rock elastic properties.

Variations in the intrusion attitude are commonly thought to represent local rotations of the principal stress axes. This is based on the assumption that dilated fractures form via Mode I failure in low deviatoric stress states where $\sigma_D < 4T$, and the intrusion lies in the σ_1-σ_2

360 plane, and normal to the σ_3 axis. Hence, areas that host several intrusion sets are interpreted to represent discrete and separate intrusive events (e.g., Delaney and Gartner, 1997). This applies particularly to intrusions that form as a result of magma chamber overpressure, where σ_1-stress trajectories emanate away from a magma chamber with an approximate conical geometry (Gudmundsson, 2006; Martí and Geyer, 2009). Whether the σ_1 trajectories are low-angle (sill-

365 like) or high angle (dike-like), they can be locally modified by pre-existing structures and host rock mechanical properties (Gudmundsson, 2006). The radial distribution of the σ_1 trajectories implies that sheets of opposing dip direction that form during the same magmatic event cannot cross-cut each other. Sills in the SRSVF, however, display bimodal (conjugate) dip patterns, across the metre- to kilometre scale, with mutual cross-cutting relationships and consistent

370 vertical opening directions, indicating that these sills *are not* cone sheets, and they *were not* the result of local stress reorientations. Our study suggests that intrusions of various attitudes

17

may form *simultaneously* (i.e. within the same magmatic episode), as a result of emplacement coeval with a high deviatoric far field stress state (e.g., Walker, 2016; Walker et al., 2017). This has particularly important implications for regions that may not exhibit mesoscopic or larger deformation features (e.g., faults and fractures), other than intrusions, from which the paleostress may be derived.

5.2 Accommodation of shortening: comparing sills and reverse faults in the San Rafael Sub-Volcanic Field

The SRSVF is host to dikes and sills; the sills cut, and these sills cut, and are cut by, thrust (and reverse) faults that dip to the NE and SW (**Figs 5f, 8a**; Walker et al., 2017). The tThrusts, deformation bands, and gypsum veins in the region form conjugate sets (**Fig. 5d-i**), which record a coaxial horizontal shortening and vertical thickening (Walker et al., 2017). Right Dihedra paleostress analysis (using the method of Delvaux and Sperner, 2003) of the thrust faults and deformation bands data for in the San Rafael shows a close correlation with the derived calculated stress state results for sills, with an angular mismatch between the principal stress axes of ~4°, and; ϕ-values calculated for the faults are lower than for the sills, atof 0.53-0.56 (**Fig. 5h, i**). For comparison, Bingham analyses (Yamaji, 2016) of the local sill contact data derives an average ϕ-value of 0.63 and principal stress axes creating a 6° angular mismatch with the opening angle and Right Dihedra models (**Fig. 8b**). To further constrain the stress ratio, and the relationship between intrusions and contractional shear structures, we input the thrust fault, deformation band, gypsum vein, and overall sill geometry pole data into mechanical models of normalized slip tendency (T_s; **Fig. 8c**) and dilation tendency (T_d; **Fig. 8d**). Although typically used to assess the reactivation potential of pre-existing structures in a present-day stress state (e.g. Ferrill et al., 1999), the models can also be used to fit a paleostress state to field data (e.g. Stephens et al., 2017). Normalized slip tendency ($T_s = (\tau / \sigma_n)/ T_smax$; Morris et al., 1996) and dilation tendency ($T_d = (\sigma_1 - \sigma_n) / (\sigma_1 - \sigma_3)$; Ferrill et al., 1999) are calculated from the stresses acting on a plane, or potential plane. This can be used to predict the attitude of both potential failure planes, and pre-existing fractures that are susceptible to reactivation in a given stress state. Notably, the zone of high T_s (0.8-1.0) overlaps with the zone of high T_d (0.8-1.0), indicating suggesting a likely zone of potential extensional shearextensional-shear. To enable conjugate shear failure, we used the same differential stress of $6T$, where $T = 3$ MPa, as used previously. By fitting the zones of high slip tendency to the

combined thrust fault and deformation band data, and zones of high dilation tendency to the overall sill geometry and gypsum vein data, we were able to derive a best-fit ϕ-value of 0.65, with a horizontal NE-SW σ_1 that plots within the 6° angular mismatch. The ϕ-value is consistent with the Right Dihedra (ϕ=0.53; **Fig. 5h, i**), Bingham analysis (ϕ=0.63; **Fig. 8a**) and our opening angle models (ϕ=0.77; **Fig. 7**). The ~~combined~~ field observations combined with the~~and~~ paleostress analyses suggest~~s~~ that sill emplacement took place during a state of mild horizontal radial compression.

A key difference between the strains recorded by sills and thrusts is the dominance of dilation during sill emplacement, and compressional shear during thrusting. The range of local dips, and consistent vertical opening, suggests that the sills were emplaced by a combination of brittle failure and dilation of pre-existing structures (including thrust faults); where the fluid overpressure accommodates both shear and dilation~~al strains~~. Consistent with the interpretation of Walker et al. (2017), our field observations and mechanical model results suggest that the sills represent conjugate intrusions, which record the continuity of horizontal shortening during periods of elevated magmatic pressure.

While the opening angle of dilated fractures has been used here to characterise the paleostress state during dilation of *pre-existing* cohesionless fractures, we envisage that it could also be applied to ~~tensile~~ extension or ~~extensional shear~~extensional-shear fractures, formed via failure of intact rock. In these cases, we would expect the fracture network to resemble a mesh structure (e.g. Sibson, 1996), which~~to~~ comprise~~s~~ ~~of~~ predominantly parallel (Mode I), ~~or low-angle~~and bimodal (conjugate extensional-shear) fractures,~~)~~ which~~intrusions,~~ dip at a low angle to σ_1, with opening angles of <20° (e.g. Hancock, 1985; Ramsey & Chester, 2004). ~~Failure of intact rock requires a higher fluid pressure than for reactivation of pre-existing structures. As such, although our models calculate the stress state and stress ratio, the derived estimates of driving fluid pressure ratio would be minimum values, and not truly representative of the fluid pressure required for emplacement via intact rock failure.~~ Importantly, the models presented in this study can be used to determine whether intrusive suites record changes in the tectonic stress state, or to identify fluid pressure pulses of varying magnitude in a single governing far-field stress state. These attributes have significant implications for improving our understanding of the development of past and present-day magmatic systems.

19

8̶6̲ ̲ Conclusions

Our mechanical models build upon the work of Delaney et al. (1986) and Jolly and Sanderson (1997) to use fracture geometry and opening angles to derive the principal stress axes during sill emplacement, and provide crucial new constraints on the stress state and fluid pressure, applicable to dikes, sills, and veins. The geometry of sills in the SRSVF record a continuous horizontal shortening̶d̶e̶f̶o̶r̶m̶a̶t̶i̶o̶n̶ that is otherwise accommodated by contractional faults in the area. Contoured regions on stereonets for opening angles suggest that in a high deviatoric stress state, it should be relatively rare for intrusions to be purely Mode I structures. In such settings, it should be commonplace for intrusions to accommodate a component of shear during their emplacement. Our opening angle model is particularly useful in determining paleostress states for regions where there is little brittle deformation (i.e. faulting), other than intrusions, and it may therefore present a useful and important tool in tectonic and magmatic studies.

References

Airoldi, G., Muirhead, J. D., White, J. D. L., and Rowland, J.: Emplacement of magma at shallow depth: insights from field relationships at Allan Hills, south Victoria Land, East Antarctica, Antarct. Sci., 23, 03, 281-296, doi: 10.1017/s0954102011000095, 2011.

465   Anderson, E. M.: The dynamics of faulting and dike formation with applications to Britain, Edinburgh, Oliver and Boyd., 1951.

Baer, G.: Mechanisms of dike propagation in layered rocks and in massive, porous sedimentary rocks, Journal of Geophysical Research, 96, B7, 11911, doi: https://doi.org/10.1029/91JB00844, 1991.

470

Baer, G., Beyth, M., and Reches, Z. E.: Dikes emplaced into fractured basement, Timna Igneous Complex, Israel, J. Geophys. Res.-Solid Earth., 99, B12, 24039-24050, doi: 10.1029/94JB02161, 1994.

Brenner, S. L., and Gudmundsson, A: Arrest and aperture variation of hydrofractures in layered
475   reservoirs, Geol. Soc. London Spec. Publ., 231, 117-128, 2004.

Delaney, P. T., and Gartner, A. E.: Physical processes of shallow mafic dike emplacement near the San Rafael Swell, Utah, Geol. Soc. Am. Bull., 109, 9, 1177-1192, doi: 10.1130/0016-7606(1997)109<1177:pposmd>2.3.co;2, 1997.

480   Delaney, P. T., Pollard, D. D., Ziony, J. I., and McKee, E. H.: Field relations between dikes and joints: Emplacement processes and paleostress analysis, J. Geophys. Res., 91, B5, 4920, doi: 10.1029/JB091iB05p04920, 1986.

Delvaux, D., and Sperner, B.: New aspects of tectonic stress inversion with reference to the TENSOR program, Geol. Soc. London Spec. Publ., 212, 1, 75-100. doi:
485   10.1144/gsl.sp.2003.212.01.06, 2003.

Eide, C. H., Schofield, N., Jerram, D. A., and Howell, J. A.: Basin-scale architecture of deeply emplaced sill complexes: Jameson Land, East Greenland, J. Geol. Soc., 174, 1, 23-40, doi:10.1144/jgs2016-018, 2016.

England, R. W.: The early Tertiary stress regime in NW Britain: evidence from the patterns of
490   volcanic activity: Geol. Soc. London Spec. Publ., 39, 1, 381-389, doi: 10.1144/gsl.sp.1988.039.01.33, 1988.

Ferrill, D. A., Winterle, J., Wittmeyer, G., Sims, D., Colton, S., Armstrong, A., and Morris, A. P.: Stressed Rock Strains Groundwater at Yucca Mountain, Nevada., GSA Today, 9, 5, 1-8, 1999.

495   Fossen, H.: Structural Geology, Cambridge University Press, 2010.

Gaffney, E. S., Damjanac, B., and Valentine, G. A.: Localization of volcanic activity: 2. Effects of pre-existing structure, Earth and Planetary Science Letters., 263, 3-4, 323-338, doi:10.1016/j.epsl.2007.09.002, 2007.

500   Gartner, A. E.: Geometry, emplacement history, petrography, and chemistry of a basaltic intrusive complex, San Rafael and Capitol Reef Areas, Utah., U.S. Geological Survey Open-File Report, p. 86-81, 1986.

Gudmundsson, A.: Emplacement and arrest of sheets and dikes in central volcanoes, J. Volcanol. Geoth. Res., 116, 3–4, 279-298, doi: http://dx.doi.org/10.1016/S0377-
505   0273(02)00226-3, 2002.

Gudmundsson, A.: How local stresses control magma-chamber ruptures, dike injections, and eruptions in composite volcanoes, Earth-Sci. Rev., 79, 1-2, 1-31, doi: 10.1016/j.earscirev.2006.06.006, 2006.

Gudmundsson, A.: Deflection of dikes into sills at discontinuities and magma-chamber
510   formation, Tectonophysics., 500, 1-4, 50-64, doi: 10.1016/j.tecto.2009.10.015, 2011a.

Gudmundsson, A.: Rock Fractures in Geological Processes, New York, Cambridge University Press., 2011b.

Hancock, P. L.: Brittle microtectonics: principles and practice, Journal of Structural Geology, 7, 437-457, 1985.

515

Hoek, J. D.: A classification of dike-fracture geometry with examples from Precambrian dike swarms in the Vestfold Hills, Antarctica, Geologische Rundschau., 80, 2, 233-248, doi: 10.1007/BF01829363, 1991.

Jolly, R. J. H., and Sanderson, D. J.: A Mohr circle construction for the opening of a pre-
520   existing fracture: J Struct Geol., 19, 6, 887-892. doi: http://dx.doi.org/10.1016/S0191-8141(97)00014-X, 1997.

~~Kavanagh, J. L., Menand, T., and Sparks, R. S. J.: An experimental investigation of sill formation and propagation in layered elastic media, Earth Planet. Sci. Lett., 245, 3-4, 799-813, doi: 10.1016/j.epsl.2006.03.025, 2006.~~

525   Levander, A., Schmandt, B., Miller, M.S., Liu, K., Karlstrom, K.E., Crow, R.S., Lee, C.T., and Humphreys, E.D.: Continuing Colorado Plateau uplift by delamination-style convective lithospheric downwelling, Nature., 472, 7344, 461–465, doi: 10 .1038 /nature10001, 2011.

Magee, C., Jackson, C. A. L., and Schofield, N.: The influence of normal fault geometry on
530   igneous sill emplacement and morphology, Geology, 41, 407-410, 2013.

Magee, C., Muirhead, J. D., Karvelas, A., Holford, S. P., Jackson, C. A. L., Bastow, I. D., Schofield, N., Stevenson, C. T. E., McLean, C., McCarthy, W., and Shtukert, O.: Lateral magma flow in mafic sill complexes, Geosphere., 12, 3, 809-841, doi: 10.1130/ges01256.1, 2016

Malthe-Sørenssen, A., Planke, S., Svensen, H., and Jamtveit, B.: Formation of saucer-shaped sills, Geological Society, London, Special Publications, 234, 215-227, 2004.

Martí, J., and Geyer, A.: Central vs flank eruptions at Teide–Pico Viejo twin stratovolcanoes (Tenerife, Canary Islands): J. Volcanol. Geoth. Res., 181, 1, 47-60, doi: http://dx.doi.org/10.1016/j.jvolgeores.2008.12.010, 2009.

Martínez-Poza, A. I., Druguet, E., Castaño, L. M., and Carreras, J.: Dike intrusion into a pre-existing joint network: The Aiguablava lamprophyre dike swarm (Catalan Coastal Ranges), Tectonophysics., 630, 75-90. doi: https://doi.org/10.1016/j.tecto.2014.05.015, 2014.

Morris, A., Ferrill, D. A., and Henderson, D. B.: Slip-tendency analysis and fault reactivation, Geology., 24, 3, 275-278, doi: 10.1130/0091-7613(1996)024<0275:STAAFR>2.3.CO;2, 1996.

Muirhead, J. D., Airoldi, G., White, J. D. L., and Rowland, J. V.: Cracking the lid: Sill-fed dikes are the likely feeders of flood basalt eruptions: Earth Planet. Sci. Lett., 406, 187-197, doi: 10.1016/j.epsl.2014.08.036, 2014.

Peterson, F.: A revision of units in the San Rafael Group and the Morrison Formation, U.S. Geological Survey., 1988.

Ramsey, J. M. and Chester, F. M.: Hybrid fracture and the transition from extension fracture to shear fracture, Nature, 428, 63-66, 2004.

Richardson, J. A., Connor, C. B., Wetmore, P. H., Connor, L. J., & Gallant, E. A.: Role of sills in the development of volcanic fields: Insights from lidar mapping surveys of the San Rafael Swell, Utah, Geology., 43, 11, 1023-1026, doi:10.1130/G37094.1, 2015.

Rubin, A. M.: Propagation of magma filled cracks: Annu. Rev. Earth Planet. Sci., 23, 287-336, 1995.

Sato, K., Yamaji, A., and Tonai, S.: Parametric and non-parametric statistical approaches to the determination of paleostress from dilatant fractures: Application to an Early Miocene dike swarm in central Japan, Tectonophysics., 588, 69-81, doi: http://dx.doi.org/10.1016/j.tecto.2012.12.008, 2013.

Sibson, R. H.: Structural permeability of fluid-driven fault-fracture meshes, Journal of Structural Geology, 18, 1031-1042, 1996.

23

570 Sibson, R. H.: Brittle-failure controls on maximum sustainable overpressure in different tectonic regimes: AAPG Bulletin., 87, 6, 901-908, doi: 10.1306/01290300181, 2003.

Sibson, R. H.: Reverse fault rupturing: competition between non-optimal and optimal fault orientations, Geol. Soc. London Spec. Publ., 367, 1, 39-50, doi: https://doi.org/10.1144/SP367.4, 2012.

575 Stephens, T. L., Walker, R.J., Healy, D., Bubeck, A., England, R.W., McCaffrey, K. J. W.: Igneous sills record far-field and near-field stress interactions during volcano construction: Isle of Mull, Scotland, Earth Planet. Sci. Lett., 478, 159-174, doi: https://doi.org/10.1016/j.epsl.2017.09.003, 2017.

Thyng, K.M., Greene, C.A., Hetland, R.D., Zimmerle, H.M., DiMarco, S.F.: True colors of
580 oceanography: Guidelines for effective and accurate colormap selection, Oceanography., 29, 9-13, doi: http://dx.doi.org/10.5670/oceanog.2016.66, 2016.

Walker, G. P. L.: Re-evaluation of inclined intrusive sheets and dikes in the Cullins volcano, Isle of Skye: Geol. Soc. London Spec. Publ., 76, 489-497, 1993.

Walker, R. J.: Controls on transgressive sill growth, Geology., 44, 2, 99-102, doi:
585 10.1130/g37144.1, 2016.

Walker, R. J., Healy, D., Kawanzaruwa, T. M., Wright, K. A., England, R. W., McCaffrey, K. J. W., Bubeck, A. A., Stephens, T. L., Farrell, N. J. C., and Blenkinsop, T. G.: Igneous sills as a record of horizontal shortening: The San Rafael subvolcanic field, Utah, Geol. Soc. Am. Bull., 129, 9-10, 1052-1070. doi: 10.1130/b31671.1, 2017.

590 Yamaji, A.: Genetic algorithm for fitting a mixed Bingham distribution to 3D orientations: a tool for the statistical and paleostress analyses of fracture orientations, Island Arc., 25, 1, 72-83, doi: 10.1111/iar.12135, 2016.

Yamaji, A., Sato, K., and Tonai, S.: Stochastic modeling for the stress inversion of vein orientations: Paleostress analysis of Pliocene epithermal veins in southwestern Kyushu,
595 Japan: J Struct Geol., 32, 8, 1137-1146, doi: https://doi.org/10.1016/j.jsg.2010.07.001, 2010.

600
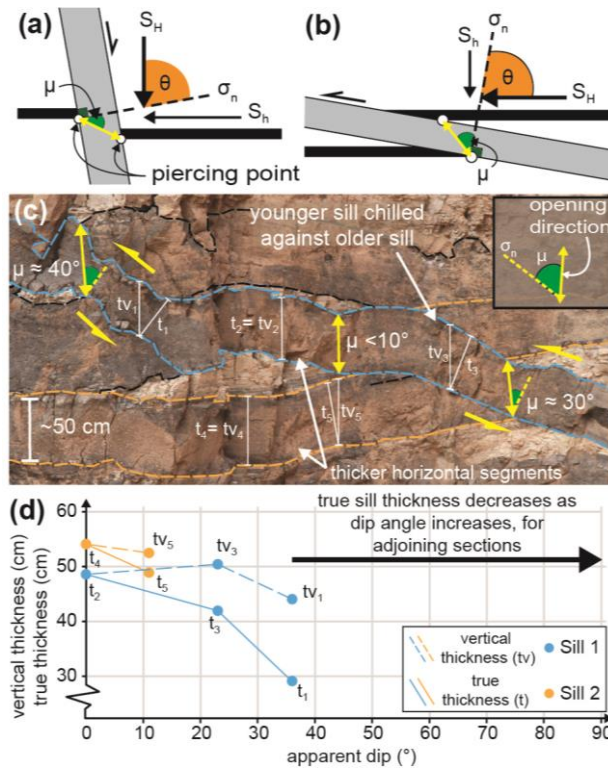
Figure 1. Schematic diagrams to show the dilation direction (yellow arrow) and opening angle (μ) of fractures in different stress ~~states~~regimes: **(a)** ~~normal~~ normal-fault regime (where $S_H = \sigma_v$); **(b)** ~~thrust~~ thrust-fault regime (where $S_h = \sigma_v$); the plane attitude is described by θ, the angle between the normal stress and the maximum stress. **(c)** Example of cross-cutting sills; the middle sill (outlined in blue) shows a consistent vertical opening direction: Mode I opening on horizontal planes, and ~~extensional shear~~extensional-shear opening on inclined planes. **(d)** Graph showing changes in vertical thickness, tv, and true thickness, t, with changes of apparent dip, for the sills shown in (c).
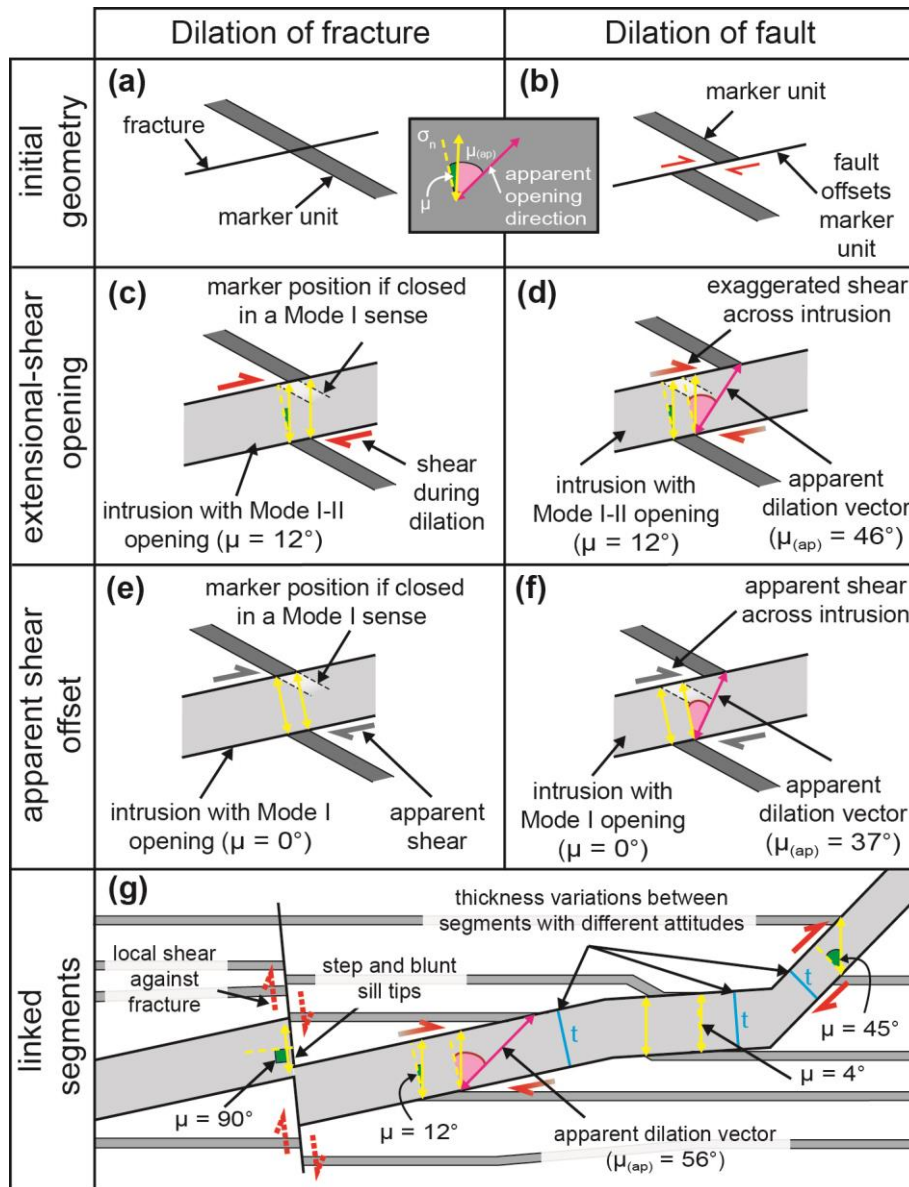
Figure 2. Figure 2. Schematic diagrams to show the relationship between opening mode and apparent shear. **(a-b)** Initial pre-intrusion geometries with a marker unit oblique to the fracture/ fault plane. **(c-d)** ~~Extensional shear~~Extensional-shear dilation of a pre-existing fracture and fault. **(e-f)** Mode I dilation of a pre-existing fracture and fault, creating an apparent shear offset. **(g)** Dilation directions and opening angles along linked segments can be used to infer the true dilation direction and fluid pressure during intrusion. μ(ap) = apparent opening angle.
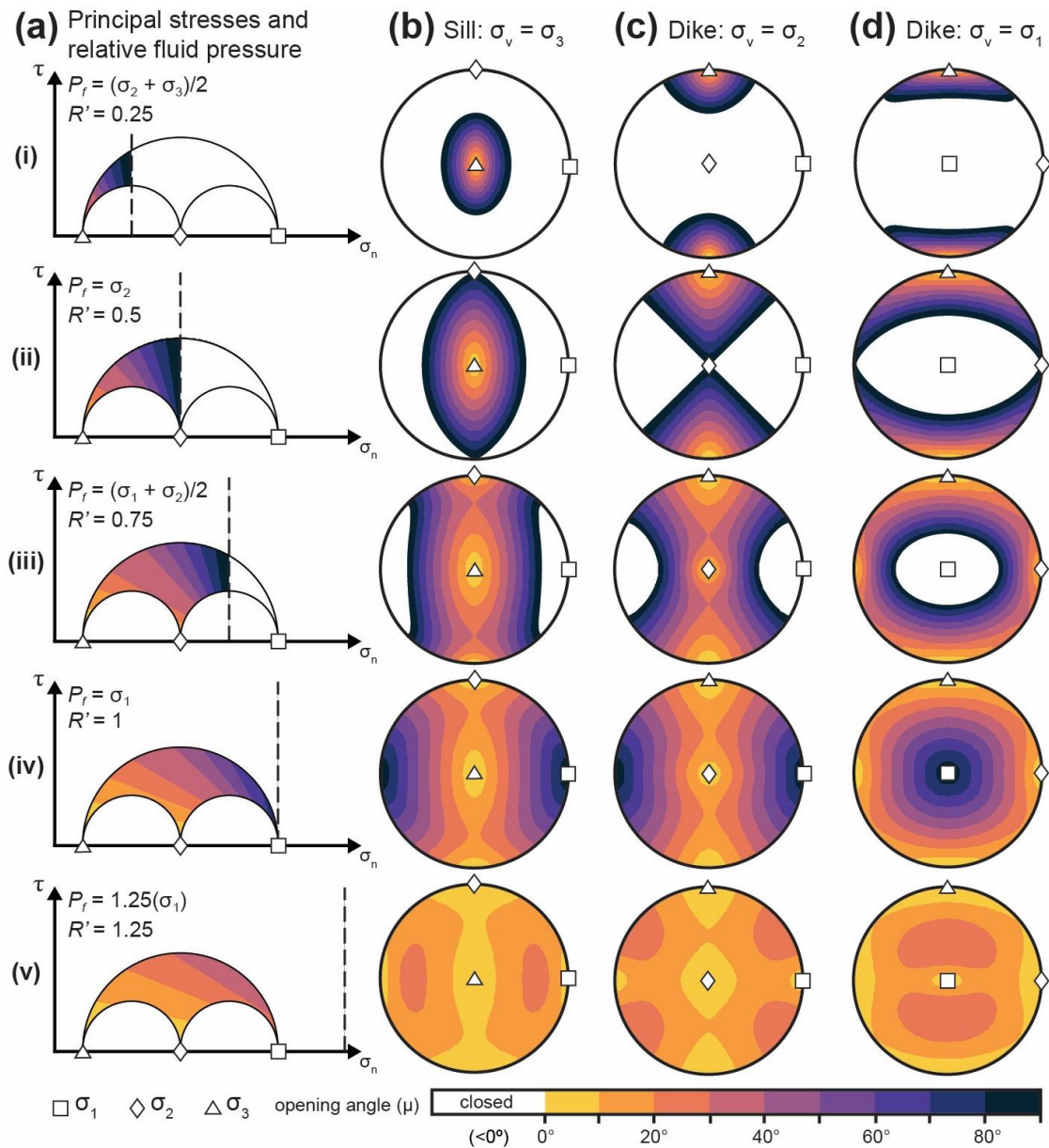
Figure 3. Mechanical models showing contoured fracture-opening angles for various stress and fluid pressure conditions, using the equation from Delaney et al. (1986), projected onto lower hemisphere, equal area stereonets and Mohr Circles (colour scheme from Thyng et al., 2016). The dashed line on the Mohr Circles indicates the fluid pressure magnitude. Five increments of fluid pressure (**a**$_{i-v}$) have been modelled with three stress states: **(b)** ~~Thrust~~ thrust-fault regime~~:~~ ($\sigma_v = \sigma_3$); **(c)** strike-slip regime ($\sigma_v = \sigma_2$); **(d)** ~~normal~~ normal-fault regime ($\sigma_v = \sigma_1$). Colour contours correspond to pole-to planes. Poles that plot in the yellow zone (where $\mu = 0\text{-}10°$) will display approximately plane-normal opening, poles with larger opening angles will display extensional-shear dilation and have a smaller true thickness than adjoining segments that plot in the yellow zone.

. ~~The dashed line on the Mohr Circles indicates the fluid pressure magnitude.~~
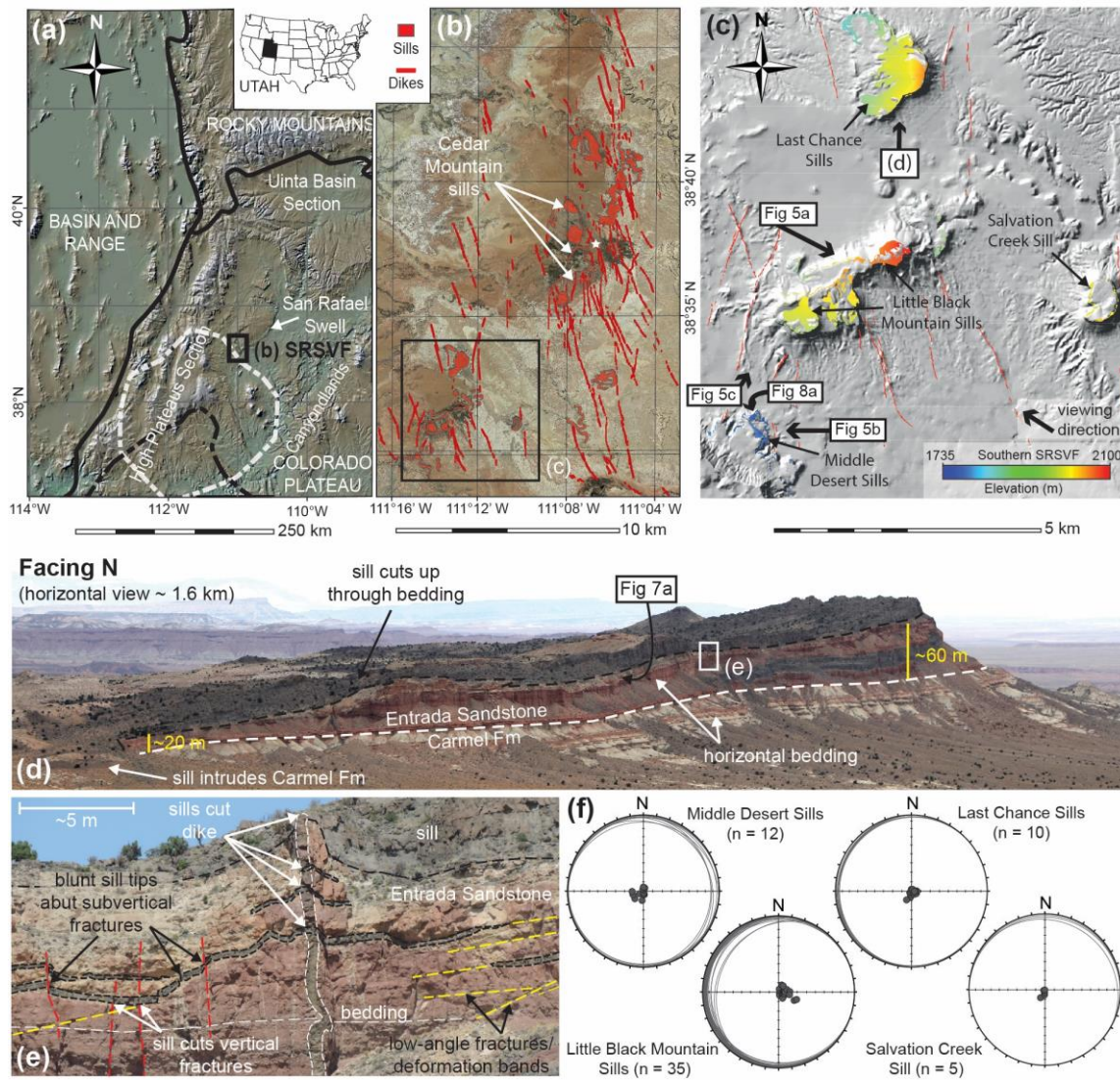
Figure 4. Location maps for the San Rafael Sub-Volcanic Field in Utah amended from Walker et al. (2017). **(a)** Digital elevation Model for Utah, showing major structural and depositional areas of the Colorado Plateau. Solid black line shows province boundaries. Dashed black line is a region of lower-crustal delamination and crustal thinning detailed in Levander et al. (2011); dashed white line is their outline of a downwelling body at 200 km depth, estimated from body wave tomography. **(b)** Aerial imagery for the San Rafael Sub-Volcanic Field (SRSVF) highlighting location and distribution of intrusive bodies; the white star marks the Cedar Mountain sill studied by Richardson et al. (2015). **(c)** Hillshaded digital elevation models for thick sills in the southern SRSVF, coloured to show extrapolated elevation data for sill top contacts (modified from Walker et al., 2017). **(d)** Field photograph of the Last Chance Sills, which transgress through the stratigraphy; the upper sill cuts across the Carmel-Entrada Formation boundary. **(e)** Sills cut dike and cut, and abut against, subvertical fractures (sills outlined in black, dike in white). **(f)** Lower hemisphere stereographic projections show sill top contact polygon attitudes (extrapolated from c) as great circles, and poles to planes for each sill system (data from Walker et al., 2017).
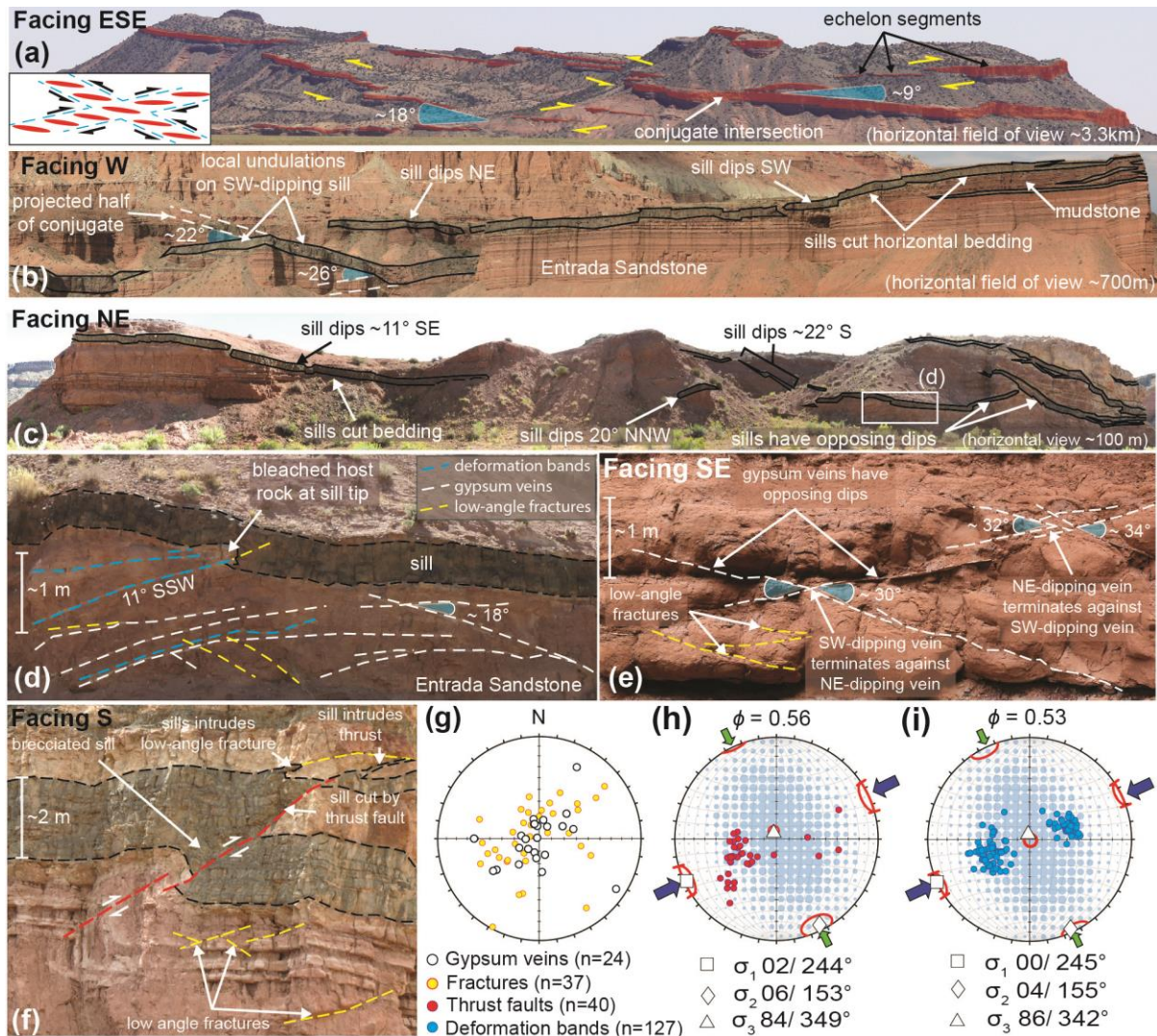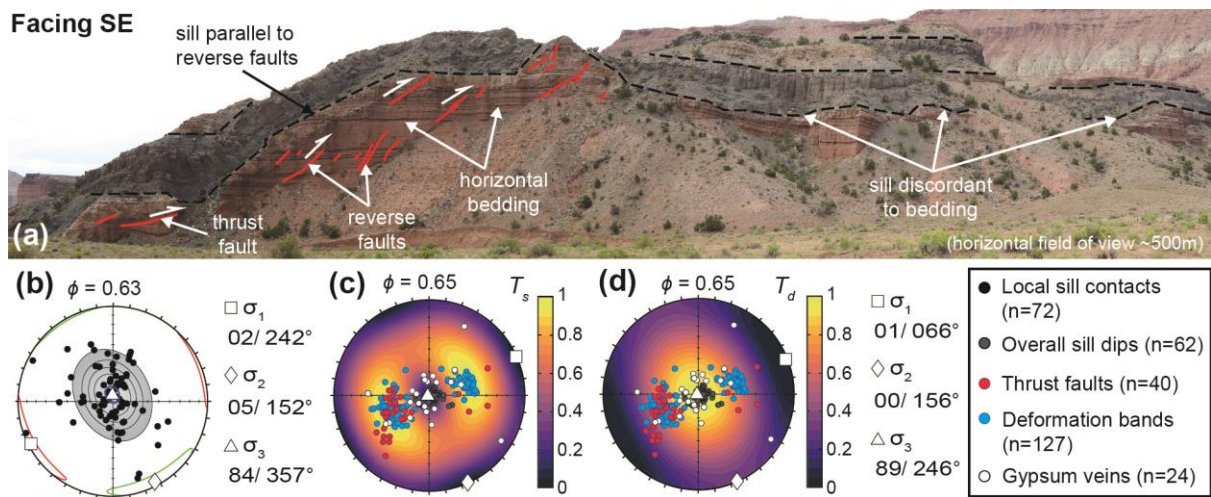
Figure 5. Sill geometry and paleostress analyses of deformation structures in the San Rafael. **(a)** km-scale segmented sills show en-echelon stepping consistent with conjugate faults (sills shaded red). Inset shows schematic interpretation. **(b)** 100 m scale sills showing NE and SW dips (sills outlined in black). **(c)** <100 m scale sills with bimodal dips (sills outlined in black). **(d)** Deformation bands and low-angle fractures parallel gypsum veins. **(e)** Gypsum veins with conjugate geometries. **(f)** Sill intruding and cut by a thrust fault and low angle fractures (sills outlined in black). **(g-i)** Lower hemisphere equal-area projections, showing: **(g)** gypsum veins and fractures, **(h)** thrust faults, and **(i)** deformation band data; principal stress axes calculated for **(h)** and **(i)** using the Right Dihedron method (Delvaux and Sperner, 2003). Calculated stress axes given as plunge/ trend measurements, ϕ-value is the stress ratio ($\sigma_2 - \sigma_3 / \sigma_1 - \sigma_3$).
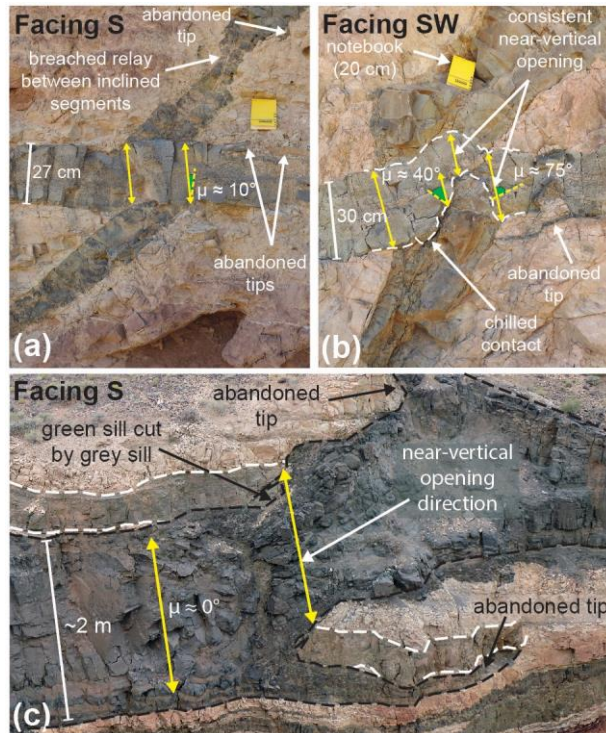
Figure 6. Sill-sill cross-cutting relationships. **(a)** Younger horizontal sill maintains a constant thickness when cutting older sill. **(b-c)** Inclined sill sections are thinner than horizontal sections. All sills show near-vertical opening directions, regardless of attitude.
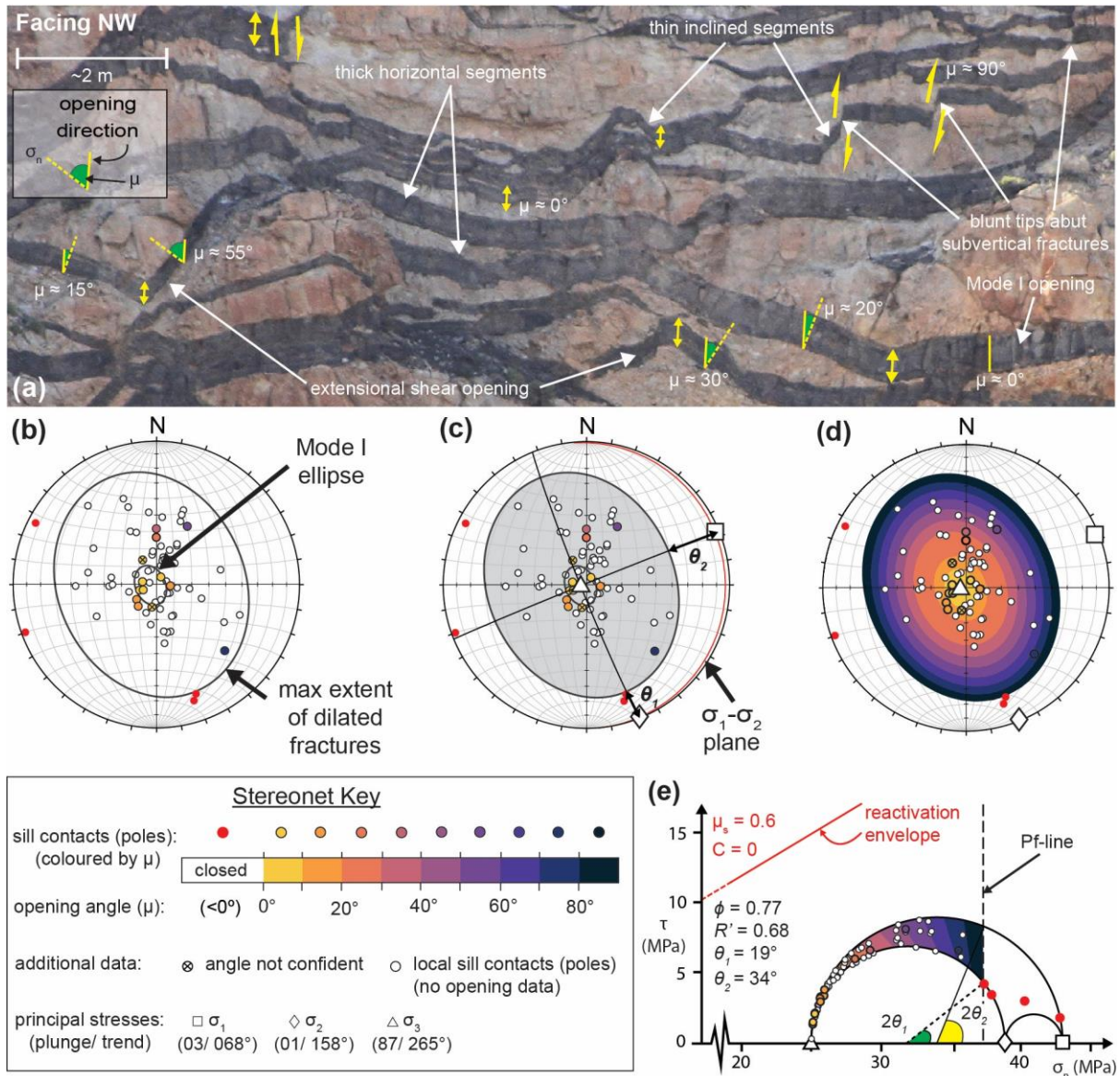
Figure 7. The opening-angle mechanical model. **(a)** Field example of thin sills (<1m thick) displaying a range of local contact dips, and a consistent vertical opening. **(b)** Lower hemisphere, equal area stereonet with local sill contacts plotted as poles to planes, coloured relative to their opening angle, with Mode I and total dilational ellipses constructed. **(c)** Determination of principal stress axes and θ angles. **(d)** Mechanical model results using the stress ratio and driving pressure (ϕ=0.77, R'=0.68; see text for details) derived from **(c)**. **(e)** 3D Mohr circle showing how θ_1 and θ_2 can be used to calculate relative fluid pressure; Mohr Circle is colour contoured for values of μ, local sill contacts are plotted as poles and coloured by their opening angle.

Figure 8. Sill geometry and paleostress analyses of deformation structures in the San Rafael. **(a)** Field example for comparison between sill and thrust fault geometry. **(b-d)** Lower hemisphere equal-area projections with calculated stress axes given as plunge/ trend measurements: **(b)** Local sill-host rock contact data, Bingham analysis (Yamaji et al., 2016) used to calculate principal stress axes, shown with 95% confidence regions and density contours (shaded region). **(c)** and **(d)** are mechanical models contoured for slip tendency (T_s) and dilation tendency (T_d), respectively.